Extension of Compact TLM Air-Vent Model on Rectangular and Hexagonal Apertures

Nebojsa Doncov, Bratislav Milovanovic, and Zoran Stankovic

Faculty of Electronic Engineering
University of Niš, Aleksandra Medvedeva 14, 18000 Niš, Serbia
nebojsa.doncov@elfak.ni.ac.rs, bata@elfak.ni.ac.rs, zoran.stankovic@elfak.ni.ac.rs

***Abstract*—** Compact transmission line matrix (TLM) air-vent model extension, to allow for a computationally efficient modelling of airflow arrays with rectangular or hexagonal apertures, even in the case of significant thickness of a supporting metal panel, is presented. An empirically derived model is introduced as an equivalent circuit into an otherwise coarse TLM mesh to account for the electromagnetic (EM) presence of apertures. The model accuracy and efficiency are validated on several characteristic electromagnetic compatibility (EMC) examples.

***Index Terms* —** Empirical air-vent model, rectangular and hexagonal apertures, TLM method.

I. INTRODUCTION

Differential numerical techniques, such as the finite-difference time-domain (FD-TD) [1] and the transmission line matrix (TLM) [2], are common tools for computational analysis of numerous electromagnetic (EM) and electromagnetic compatibility (EMC) problems. However, when attempting to apply these methods, working usually in the time-domain, to describe complex practical systems, treatment of geometrically small but electrically important features, often found on these systems, presents a challenging and time-consuming task. A conventional solution of employing a very fine mesh to model these features in an otherwise large modelling space leads in some cases to a prohibitively large number of nodes and time steps. Therefore, enhancements to these techniques are required to allow for an efficient simulation of realistic multi-scale EM and EMC problems.

For some of the fine features, such as wires and slots, few enhancements to the FD-TD method [3, 4] and the TLM method [5-7] have been developed in the past. As far as the TLM method is concerned, these so-called compact models have been implemented in the form of an additional one-dimensional transmission line network running through a tube of regular nodes, allowing accounting for the EM presence of wires and slots without applying a very fine mesh around them. Compared with the conventional approach, these models yield a dramatic improvement in the computer resources required. A different type of solution has been presented in [8] in the form of several modified TLM nodes developed to accurately model the fast variation of the EM field around sharp conducting regions by coarse mesh.

Airflow aperture arrays or air-vents, often found on equipment enclosures for ventilation purposes, fall into the category of fine features. Their presence can significantly increase emission and decrease shielding effectiveness of the box [9]. Again, if conventional FD-TD and TLM as effective volume-based methods are used without any enhancement (e.g. compact model or modified node), an extremely fine mesh is required to accurately capture the strong variation of the EM field across each aperture dimension and depth of the supporting panel. Therefore, it has a cost that prediction of enclosure performances at the design stage, due to presence of air-vents, can be computationally very expensive [10].

In recent years, enhancements of the TLM method, based on **Z**-transform approach, have been done and applied, among other things, to model air-vents [11]. In parallel with this approach, a simple compact model solution of air-vent for square and circular apertures has been

developed and presented in [10]. This efficient solution, developed especially for air-vents, is easy for implementation and it does not require a modification of standard TLM symmetrical condensed node (SCN) and its scattering procedure. It was based on the insertion of equivalent circuit with an empirically found inductive element into an otherwise course mesh. The equivalent circuit model is often used for EM and EMC analyses, but in [10] it was implemented into the time-domain solver. Both approaches take into account the EM presence of air-vents using computational cells larger than the individual apertures and achieving significant savings in memory and run-time in comparison with the conventional TLM approach. In addition, the approach in [10] has been enhanced to allow modelling of square and circular air-vents for significant perforation depth and at higher frequencies, verified only on one artificial example of plane wave propagation through circular aperture array in a thick metal panel [12].

In this paper, the approach described in [12] is extended on air-vents with rectangular and hexagonal apertures, found on equipment boxes as often as square or circular apertures. The real usefulness of being able to model, for an example, rectangular perforations comes from the case of simulating a box full of complicated equipment. In that case, it is unknown what the dominant polarization will be; the polarization is off-axis or is different at different parts of the vent. Thus, this model will produce much more accurate results than the compact square air-vent model used sometimes to approximately describe an array of rectangular apertures. The modelling of air-vents with rectangular and hexagonal apertures is described in details in the paper.

All the models are incorporated into a three-dimensional (3D) SCN TLM mesh and implemented in 3D TLM*scn* solver, designed at the Microwave Lab at the Faculty of Electronic Engineering in Nis, Serbia. This TLM solver has been already successfully applied to many EM problems such as resonant cavity-based microwave applicators [13]. The ability of the presented models to accurately account for the EM presence of apertures, even in the case of significant perforation depth, and their run-time and memory efficiencies are successfully validated in several characteristic EMC environments. Obtained results of simulated transmission through an imperfectly shielded test enclosure with different air-vents are compared with the experimental and fine TLM SCN mesh results.

II. MODEL DESCRIPTION

Perforations on thin metal screens, for a normally incident plane wave excitation, can be treated as an inductive short on the TLM link lines used to represent a thin panel. This inductive susceptance is the simplest possible arrangement acting as a perfect short at DC and allowing transmission at higher frequencies [9]. In addition, a perforation on a metal screen may be regarded as an extremely short, highly cut-off waveguide, while in a lumped component model of such a waveguide, only shunt inductance would be significant. Therefore, current flowing down the edges of apertures on a thin metal panel can be successfully represented by this shunt inductance. However, at higher frequencies, there is a requirement to accurately capture an EM field distribution inside the aperture itself, especially if there is a significant perforation depth. An equivalent circuit containing an additional capacitive element connected in shunt with an inductive short is capable to model very deep apertures while allowing easy TLM implementation (Fig.1).

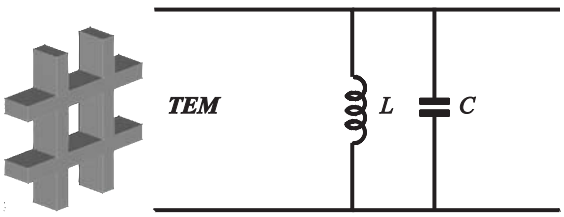

Fig. 1. Compact air-vent model based on *LC* network.

For a TEM line of characteristic impedance Z_0 with a shunt reactance X inserted at its midpoint, $X = \omega L_e$ where L_e is an equivalent inductance expressed as $L/(1- \omega^2 LC)$, the transmission coefficient is:

$$T = jX / (jX + Z_0 / 2), \qquad (1)$$

or for low frequency approximately proportional to the reactance X. It is reasonable to expect that the break frequency $f_{break}=(Z_0/2)/(2\pi L_e)$ would correspond to the cut-off frequency of the perforation and that the transmission would reduce

in proportion to the decreasing of a fractional area of the panel occupied by the perforations and increasing of panel thickness. This reduction in transmission of a perforated metal panel, being achieved by proportional reductions in L_e, obviously depends on the actual geometry of the perforations.

In order to empirically determine effective reactive parameters of a perforated panel containing rectangular or hexagonal apertures, the numerical procedure similar to the one in [12] is used. The conventional TLM method with a very fine computational mesh is applied to find the transmission coefficient of a perforated panel for a normally incident plane wave. However, in the case of rectangular apertures, as explained previously, this should be done separately for horizontal and vertical polarization. Symmetry conditions were exploited to model only one period of the perforation. The results for output of the far side of the panel, obtained for different dimensions of perforations and for different panel thicknesses (up to cross-sectional dimensions of the apertures) indicate that transmission increases slightly more than proportionally to the fractional coverage of the panel by the apertures. At the same time, transmission decreases almost exponentially with increasing the perforation depth. This can be seen from Fig. 2 and Fig. 3, taken at frequency $f = 0.2\, f_c$ where f_c is the cut-off frequency of the considered perforation.

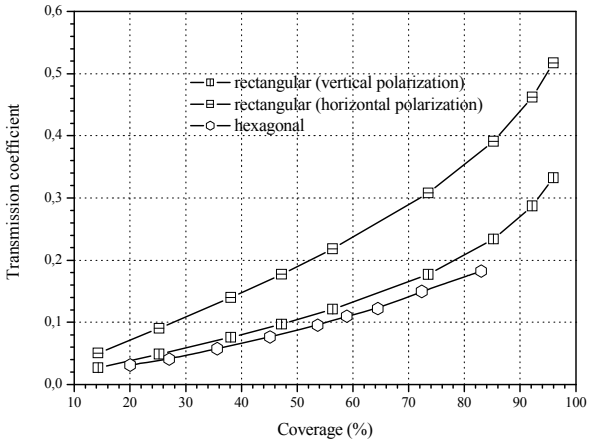

Fig. 2. Transmission versus coverage for rectangular (vertical and horizontal polarization) and hexagonal aperture.

In addition, the results for the transmission coefficient of a panel with hexagonal apertures show that this aperture can be successfully approximated with a circular aperture of equivalent radius r_e, obtained from the condition of the same coverage (Fig. 4):

$$\frac{r_e^2\pi}{p^2} = \frac{6\, l_{hex}^2\sqrt{3}/4}{p^2} \Rightarrow r_e = l_{hex}\sqrt{\frac{3\sqrt{3}}{2\pi}}, \quad (2)$$

where: l_{hex} is an edge length of regular hexagonal aperture. In order to illustrate this, transmission coefficient, obtained for a perforated plate containing either hexagonal apertures with edge length of 1 mm or circular apertures with equivalent radius of 0.909 mm, is shown in Fig. 5. The thickness of a supporting metal panel was 10% of the edge length and total coverage was 53.679 %.

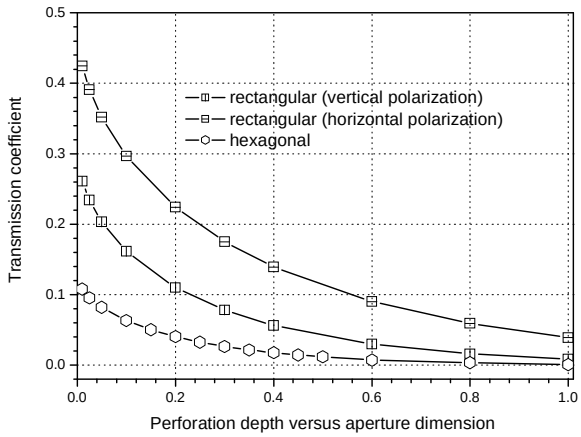

Fig. 3. Transmission versus perforation depth for rectangular (vertical and horizontal polarization) and hexagonal aperture.

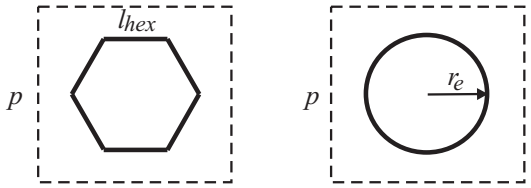

Fig. 4. a) Regular hexagonal aperture and b) its equivalent circular aperture.

Based on these results and using Eq. (1), the equivalent inductance L_e was calculated at two frequencies f_1 and f_2 chosen to bracket most of the band below perforation cut-off (e.g. f_1 =0.1 f_c and

f_2=0.8 f_c). Then, the equivalent inductance of the panel was approximated as a product of several factors that include the shape, depth, and cut-off frequency of the perforation and the panel coverage:

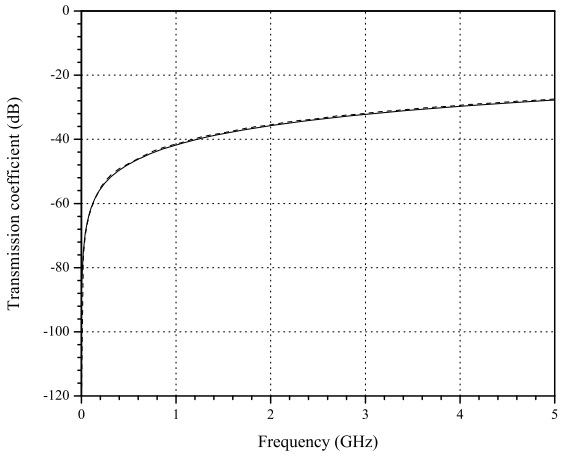

Fig. 5. Transmission coefficient of a perforated metal plate containing either hexagonal apertures of edge length l_{hex} (solid line) or circular apertures of equivalent radius r_e (dash line).

$$L_e = \text{form\_factor} * L\_\text{cutoff} * \text{coverage\_factor} * \text{depth\_factor} = A_0 * \left(\frac{Z_0/2}{2\pi f_c}\right) * \left(\sum_{i=1}^{3} A_i \text{cov}^i\right) * \text{Exp}\left(-A_4 \frac{t}{v/(2\pi f_c)}\right), \quad (3)$$

where: *cov* is the fractional area of the metal panel cut away; t is perforation depth and v is speed of light. Constants A_0, A_1, A_2, A_3, and A_4 are given in Table 1 for rectangular and hexagonal aperture shapes and for horizontal (H) and vertical (V) polarization. The previously empirically found coefficients for square and circular apertures are shown on the same table. Hexagonal and circular apertures have the same coefficients, but the value of equivalent inductance, obtained from Eq. (3), is different for these shapes due to different cut-off frequencies.

It should be said that the application of the proposed models for rectangular and hexagonal aperture shape is restricted to the range of aperture parameters that fulfill the conditions already mentioned in [12].

Table 1: Constants used in L_e approximation

	Aperture shape	A_0	A_1	A_2	A_3	A_4
L_e (f_1)	circular and hexagonal (H and V)	1.433	1.0	0.472	0	1.052
	square (H and V)	1.491	1.0	0.472	0	1.080
	rectangular (V)	4.692	0.523	-0.861	1	0.917
	rectangular (H)	4.697	0.593	-0.807	1	0.853
L_e (f_2)	circular and hexagonal (H and V)	1.741	1.946	-0.75	0	0.673
	square (H and V)	1.574	1.525	0.264	0	0.728
	rectangular (V)	5.694	0.6	-1.050	1	1.044
	rectangular (H)	8.385	0.718	-1.294	1	1.163

The model is implemented in a way that effective inductance and capacitance of the panel, L and C, are chosen so that their reactance in parallel is $2\pi fL_e$ at frequencies f_1 and f_2. For each polarization, they are implemented in traditional TLM mesh using additional short- and open-circuit stub lines, at the interface between two nodes (Fig. 6a). The scattering procedure for the aperture array can be then easily derived applying the Thevenin equivalent circuit (Fig. 6b).

Since, in general, apertures extend in two different directions, voltage pulses from both orthogonally polarized TLM link lines are coupling with the aperture. The total voltage at the interface, for a particular polarization, is:

$$V_{total} = 2\frac{V_l^i Y_l + V_r^i Y_r + V_s^i Y_s + V_o^i Y_o}{Y_l + Y_r + Y_s + Y_o}, \quad (4)$$

where: V_l^i and V_r^i are incident voltage pulses from the link lines of characteristic admittances Y_l

and Y_r, coupling with the aperture and V_s^i and V_o^i are incident voltage pulses on short and open stub lines of characteristic admittances Y_S and Y_O, respectively. Reflected voltage pulses are then:

$$\begin{aligned} V_l^r &= V_{total} - V_l^i; \quad V_r^r = V_{total} - V_r^i \\ V_s^r &= -V_{total} + V_s^i; \quad V_o^r = V_{total} - V_o^i \end{aligned} \tag{5}$$

III. NUMERICAL RESULTS

First, capability of the previously developed compact TLM air-vent model for square apertures to model perforated metal screen with significant thickness is illustrated in the characteristic EMC environment (rectangular test enclosure depicted in Fig. 7). The inside dimensions of the enclosure are: *a*=50 cm, *b*=20 cm, and *c*=40 cm. A thin (*t*=0 cm) or thick (*t*=1 cm) aluminium plate was used for the front face containing the array of square apertures, while five other enclosure pieces were with thickness 0.635 cm. The square aperture size was *l*=1 cm, with an edge-to-edge space of 0.5 cm. The number of apertures was 252. The model was excited by a long-wire feed at the back of the box which was modelled by a simple voltage source V=1 mV with 50 Ohm resistance incorporated into a single node at the feed point. The excitation had the centre conductor of the probe extended to span the width of the cavity with a 0.16 cm diameter wire, modelled using wire node [5], and terminated on the opposite cavity wall with termination of 47 Ohm. Choice of geometry, lossy material of thickness *d*=1 cm, excitation, and output was governed by experimental arrangements [14].

The compact model for square perforations was incorporated into a coarse TLM mesh (21*10*20 nodes used for enclosure modelling where Δy=Δz=2 cm, Δx=1 cm for lossy material, and 2.45 cm elsewhere). The same mesh size was used either for thin or thick front face as thickness of front wall was specified in the compact model. TLM simulation was performed, as for all other EMC examples considered in this section, on Intel Core 2 Duo PC machine with 2.66 GHz clock rate, 2 GB RAM, and 32-bits Windows XP OS. Numerical results for the electric field at point 3 m away from the box, for zero-thin and thick front face, have been compared to the experimental results given in [14] and an excellent agreement (Fig. 8) has been observed except at higher frequencies, probably due to neglecting the frequency dependant characteristics of the lossy material at the back of the box.

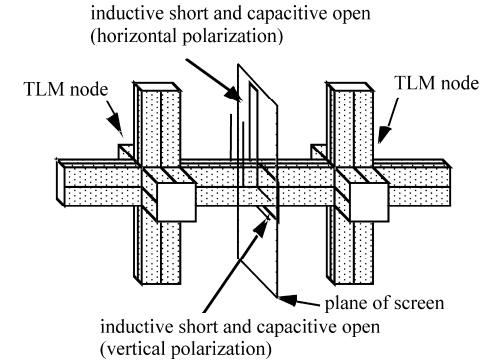

a)

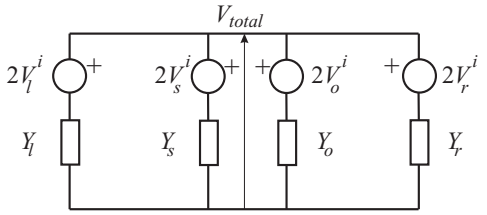

b)

Fig. 6. a) *LC* model at the interface between two TLM nodes, b) Thevenin equivalent circuit for a particular polarization.

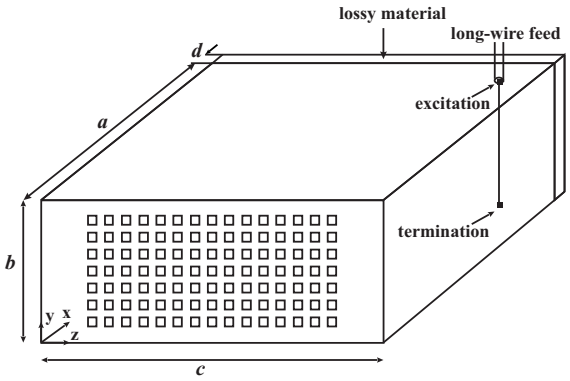

Fig. 7. Imperfectly shielded test enclosure with an array of square apertures on front face.

In reference [14], additional compensation factors, due to the insufficient number of nodes to describe the aperture, were found and applied to correct FD-TD numerical results. As compact TLM air-vent model allows for inherent modelling of the aperture shape and depth, much coarser mesh was used but no additional factors are required. Therefore, savings of two orders of magnitude in memory and run-time are achieved,

compared to the traditional fine mesh FD-TD simulation. It should be said that in the case of thick front face, where perforation depth was equal to square aperture size (t=l), experimental results were scaled according to formula $16\sqrt{\pi}(t/l)$ given in [14].

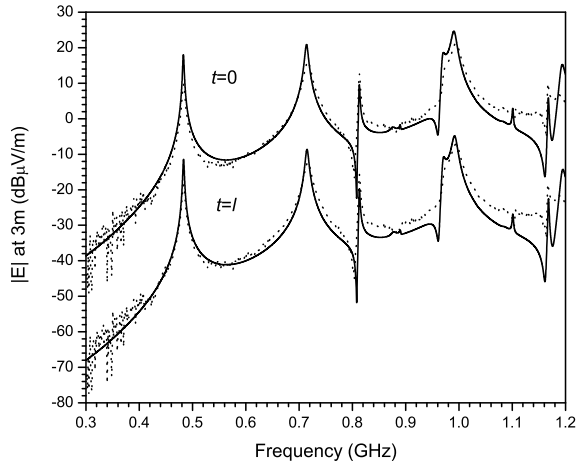

Fig. 8. Radiated electric field at 3m away from enclosure (solid line: compact air-vent model, dot line: measurements).

The developed compact TLM air-vent model for rectangular perforations has been verified simulating transmission out of an imperfectly shielded rectangular test enclosure. The dimensions of the box were: a=100 mm, b=80 mm, and c=15 mm (Fig. 9). A t=0.2 mm thin aluminium plate was used on two opposite faces of the box as a supporting panel for the array of rectangular apertures. The dimensions of rectangular perforation were 7.2 mm in x- and 4 mm in z-direction. Edge-to-edge aperture spacing was 1.8 mm in x- and 1 mm in z-direction. The number of apertures for each array was 33 giving a total coverage of 63.36%. The box was excited by a straight wire placed inside the box (position 1).

The compact model was applied on a relatively course mesh (61*44*10 nodes used for enclosure modelling where Δx=1.639 mm, Δy=1.818 mm, and Δz=1.5 mm). The total run-time was 1.5 min, while allocated memory was 33 Mb (see Table 2). Then, a fine mesh of 112*49*16 is applied to model enclosure with these airflow arrays using only conventional TLM routines. In order to model geometry of the apertures and accurately describe EM field distribution inside and around the apertures, 8 uniform grid lines

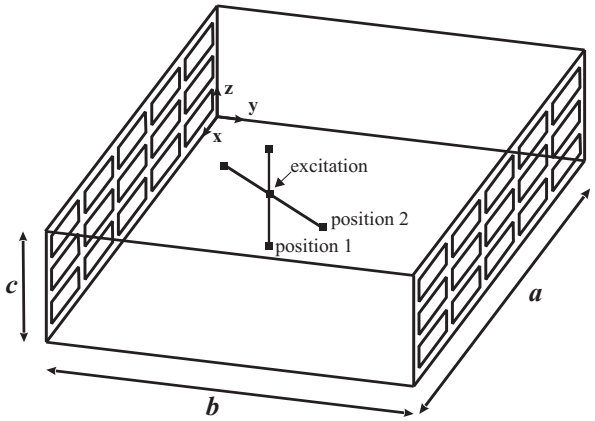

Fig. 9. Imperfectly shielded test enclosure with array of rectangular apertures on opposite faces.

along the bigger (Δx=0.9 mm), and 4 uniform grid lines along the smaller dimension of rectangular apertures (Δz=1 mm) were used to describe their cross-section. The same grid resolution in each direction was used to describe edge-to-edge spacing. Spacing from the first and last aperture to enclosure edges were represented by two nodes of 0.7 mm in x- and one node of 0.5 mm in z-direction. Perforation depth of 0.2 mm was represented by one node. As it can be seen from Table 2, the total run time was 60 min on the same PC machine with more than two times memory resources allocation than the compact model. Electric field in front of one airflow array, obtained by these two simulations is shown in Fig. 10.

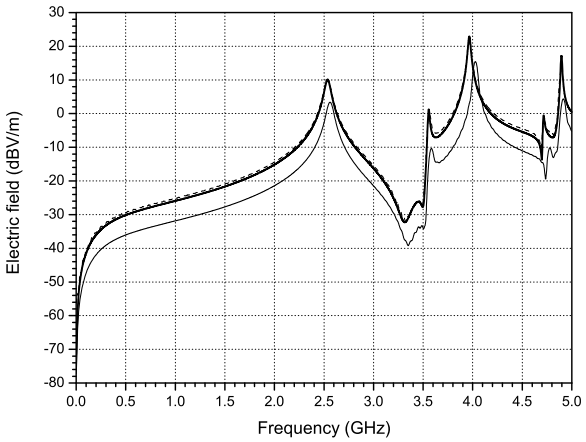

Fig. 10. Electric field in front of thin rectangular airflow array (bold solid line: compact air-vent rectangular model, thin solid line: compact air-vent square model, dash line: fine mesh).

Excellent agreement between the compact air-vent model and fine mesh results can be observed.

The result for electric field obtained by the compact square air-vent model and the same mesh size of 61*44*10 nodes for enclosure modelling is shown on the same figure. The number (60) and dimension of square apertures (4 mm) were defined in the compact model to represent the same coverage of imperfectly shielded faces as in the case of rectangular apertures. As it can be seen, these results are significantly below the fine mesh results. How for this particular case, electric field has a dominant z component, the compact square air-vent model might produce better results if we chose the dimension of square aperture equal to the bigger dimension of rectangular aperture. However, in many practical cases a box is full of complicated equipment and the dominant polarization of the EM wave at air-vents is often unknown. Also, the wave polarization might be off-axis or different at different parts of the airflow array. Thus, in cases when rectangular perforations are used for ventilation, the usefulness of being able to model them exactly is clearly obvious.

Table 2: Simulation cost of compact air vent model and fine-mesh TLM model generating numerical results shown in Figs. 10, 11, and 13

	Simulation cost	Fig.10	Fig.11	Fig.13
Compact model	run-time	1.5 min	2 min	20 sec
	allocated memory	33 Mb	35 Mb	6 Mb
Fine mesh	run-time	60 min	94 min	22 min (fm 1)
				220 min (fm 2)
	allocated memory	68 Mb	132 Mb	41 Mb (fm 1)
				154 Mb (fm 2)

To illustrate capability of describing perforations on a very thick supporting metal panel, the test enclosure from Fig. 9 was considered, but dimensions of each of the 16 rectangular perforations were 10.85 mm in x- and 5.08 mm in the z-direction with edge-to-edge spacing of 0.69 mm. Perforation depth of both air-vents was 5.2 mm. Wire feed was placed diagonally inside the box (position 2). In a fine TLM mesh with 156*49*24 nodes for enclosure modelling, 16 and 7 uniform grid lines along the bigger (Δx=0.678 mm) and along the smaller dimension of apertures (Δz=0.726 mm), respectively, were used to describe their cross-section. To capture EM field distribution inside the perforation more accurately, 26 uniform grid lines (Δx=0.2 mm) in y-direction were applied. A compact air-vent model was applied on a coarse TLM mesh of 51*41*15 nodes (Δx=1.96 mm, Δy=1.95 mm, and Δz=1 mm; mesh is slightly different than the coarse mesh for Fig. 9 due to modelling of a diagonal wire). Run-time and allocated memory for both meshes are shown in Table 2. The comparison of the results for the electric field in front of air-vents is presented in Fig. 11.

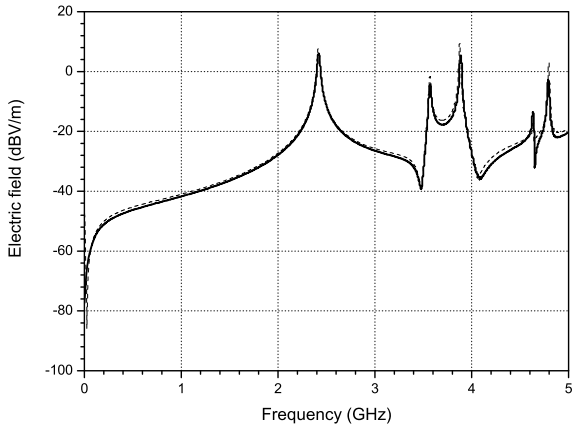

Fig. 11. Electric field in front of thick rectangular airflow array (solid line: compact air-vent rectangular model, dash line: fine mesh).

The calculation of shielding effectiveness (SE), for an aluminium enclosure with an array of hexagonal apertures covering one part of front face (Fig. 12, $a \times b \times c$=295×120×295 mm, $b_1 \times c_1$=60×190 mm), was used to verify a compact air-vent model for hexagonal apertures. The incident plane wave had an electric field polarised in y-direction. The edge length of hexagonal perforation was 6.6 mm and the number of

apertures was 20 giving a 20% total coverage of front face perforated area.

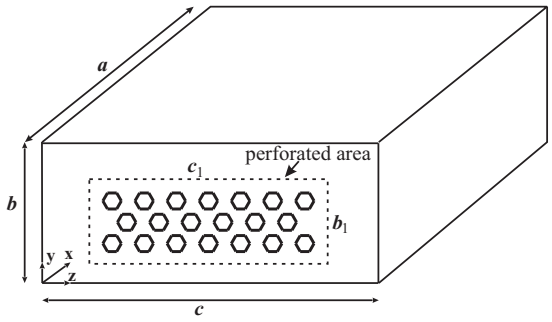

Fig. 12. Imperfectly shielded test enclosure with array of hexagonal apertures partially covering front face.

Two TLM fine meshes: fm 1 with 30*48*144 nodes and fm 2 with 39*94*244 nodes were used for enclosure modelling. Number of nodes used for each aperture cross-section dimension was 10 (fm 1) and 16 (fm 2). Also, a few more nodes in fm 2 are added in the x-direction (Δx=1.2 mm) around front face in order to more accurately account for plane wave coupling with aperture array. The compact model simulation used coarse mesh of 11*10*17 nodes to produce the similar results for SE up to 1 GHz (Fig. 13), either for front face with zero thickness (t=0 mm) or with thickness t=6 mm (described by 5 nodes in fm 2). Savings in memory and run-time, achieved by the compact model, in comparison with fine meshes for the case t=0 mm are shown in Table 2.

IV. CONCLUSION

This paper described an extension of the TLM method to allow for efficient computer modelling of EM field propagation through array of rectangular or hexagonal apertures in metal equipment boxes. It is based on insertion of equivalent circuit into otherwise coarse mesh, an approach that was often used in the area of computational electromagnetics to produce simple but accurate solutions to many EM problems. Here, this approach with empirically found elements of lumped circuit for some typical aperture shapes is applied to account for the strong variation of EM fields inside and around the apertures even in the case of significant depth of the supporting panel. Presented examples verify the efficiency of the developed equivalent circuit model with accuracy acceptable for most EMC applications. In addition, its implementation in comparison with other existing approaches requires very little modification of the existing traditional TLM code. The considered apertures are with regular shapes but it is clear that irregular apertures can be treated in a similar way with the same or more complicated circuits as well as long as the transmission coefficients are numerically available.

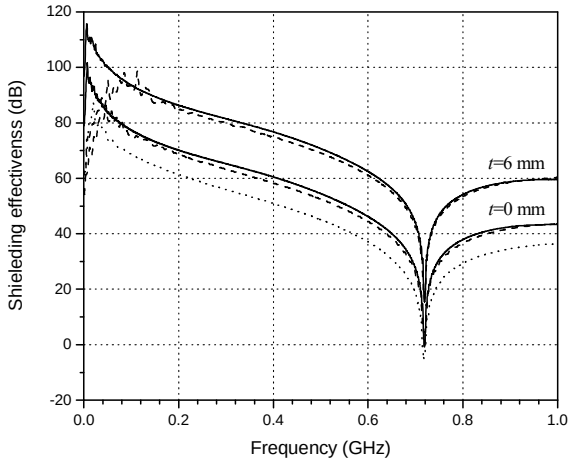

Fig. 13. SE of a metal enclosure in Fig. 12 (solid line: compact air-vent hexagonal model, dot line: fm 1, dash line: fm 2).

ACKNOWLEDGMENT

This work has been supported by the Serbian Ministry of Science under the project TR-32052.

REFERENCES

[1] K. S. Kunz and R. J. Luebbers, *The Finite Difference Time Domain Method for Electromagnetics*, CRC Press, Boca Raton, FL, 1993.

[2] C. Christopoulos, *The Transmission-Line Modelling (TLM) Method*, IEEE/OUP Series, Piscataway, NJ, 1995.

[3] F. Edelvik, "A New Technique for Accurate and Stable Modeling of Arbitrarily Oriented Thin Wires in the FDTD Method," *IEEE Trans. Electromagn. Compat.*, vol. 45, no. 2, pp. 416-423, 2003.

[4] F. Edelvik and T. Weiland, "Stable Modelling of Arbitrary Oriented Thin Slots in the FDTD

Method," *IEEE Trans. Electromagn. Compat.*, vol. 47, no. 3, pp. 440-446, 2005.

[5] A. J. Wlodarczyk, V. Trenkic, R. Scaramuzza, and C. Christopoulos, "A Fully Integrated Multiconductor Model for TLM," *IEEE Trans. Microwave Theory Tech.*, vol. 46, no. 12 pp. 2431-2437, 1998.

[6] J. Paul, C. Christopoulos, D. W. P. Thomas, and X. Liu, "Time-Domain Modeling of Electromagnetic Wave Interaction with Thin-Wires using TLM," *IEEE Trans. Electromagn. Compat.*, vol. 47, no. 3, pp. 447-455, 2005.

[7] V. Trenkic and R. Scaramuzza, "Modelling of Arbitrary Slot Structures using Transmission Line Matrix (TLM) Method," *Int. Symp. Electromagn. Compat.*, Zurich, Switzerland, pp. 393-396, 2001.

[8] J. A. Morente, J. A. Porti, H. Magan, and O. Torres, "Improved Modeling of Sharp Zones in Resonant Problems with the TLM Method," *Applied Computational Electromagnetic Society (ACES) Journal*, vol. 14, no. 2, pp. 67-71, 1999.

[9] T. Y. Otoshi, "A Study of Microwave Leakage through Perforated Flat Plates," *IEEE Trans. Microwave Theory Tech.*, vol. 20, no. 3, pp. 235-236, 1972.

[10] N. Doncov, A. J. Wlodarczyk, R. Scaramuzza, and V. Trenkic, "TLM Modelling of Perforated Metal Screens," *4th Int. Conf. Computational Electromagnetics*, Bournemouth, UK, 2002.

[11] J. Paul, V. Podlozny, and C. Christopoulos, "The Use of Digital Filtering Techniques for the Simulation of Fine Features in EMC Problems Solved in the Time Domain," *IEEE Trans. Electromagn. Compat.*, vol. 45, no. 2, pp. 238-244, 2003.

[12] N. Doncov, A. J. Wlodarczyk, R. Scaramuzza, and V. Trenkic, "Compact TLM Model of Air-Vents," *Electronics Letters*, vol. 38, no. 16, pp. 887-888, 2002.

[13] J. Jokovic, B. Milovanovic, and N. Doncov, "Numerical Model of Transmission Procedure in a Cylindrical Metallic Cavity Compared with Measured Results," *Int. Journal of RF and Microwave Computer-Aided Engineering*, vol. 18, no. 4, pp. 295-302, 2008.

[14] M. Li, J. Nuebel, J. L. Drewniak, R. E. DuBroff, T. H. Hubing, and T. P. Van Doren, "EMI from Airflow Aperture Arrays in Shielding Enclosures – Experiments, FDTD, and MoM Modelling," *IEEE Trans. Electromagn. Compat.*, vol. 42, no. 3, pp. 265-275, 2000.